SECOND-ORDER STEREOLOGY OF PROSTATIC ADENOCARCINOMA AND NORMAL PROSTATIC TISSUE

Torsten Mattfeldt, Ulrich Vogel, Hans-Werner Gottfried, Herbert Frey

Department of Pathology, University of Ulm
Oberer Eselsberg M23, D-89081 Ulm, Germany

ABSTRACT

The spatial arrangement of the epithelial tissue component was studied in prostatic cancer and in normal prostatic tissue by applying second-order stereological methods to histological sections from 20 prostatectomy specimens. Interactive segmentation of the epithelial tissue component in normal and neoplastic tissue was performed with an image analyzer. The epithelial component was considered as a stationary isotropic ergodic random closed set with positive volume fraction V_V (volume process). The covariance $C(r)$ of a volume process is the probability that two points in the reference space, separated by a line of length r, hit the process simultaneously. An unbiased estimate $\hat{C}(r)$ of the covariance of the epithelial volume component was obtained automatically from the stored images. From $\hat{C}(r)$ and the estimated volume density $\hat{V}_V$, consistent estimates of the correlation function $k(r)$, of the pair correlation function $g(r)$, of the radial distribution function $RDF(r)$ and of the reduced second moment function $K(r)$ of epithelial volume were determined. Estimation of $C(r)$ and $RDF(r)$ alone did not permit a distinction between different types of spatial arrangement of epithelium in benign and malignant tissue. Estimation of $k(r)$, $g(r)$ and $K(r)$ showed clustering of epithelial volume at short distances and repulsion at long distances. The best discrimination between benign and malignant tissue was obtained by estimation of $g(r)$. The pair correlation function indicated a partial loss of epithelial interaction in the carcinomatous tissue, which was more pronounced in cribriform than in acinar adenocarcinomas. Second-order stereology reproducibly detects architectural changes in malignant lesions of glandular organs, with $g(r)$ serving as the most useful tool.

Keywords: Image analysis, microscopy, prostate cancer, second-order statistics, stereology, stochastic geometry.

INTRODUCTION

Most stereological studies have been concerned with the estimation of characteristics (in particular, parameters) of three-dimensional structures from measurements on planar sections. Examples are the well-known "densities" (mean volume, surface area, length, and number per unit volume) of classical stereology, and the mean volume of particles. Often, the parameters represent the first moments of size distributions and are therefore denoted as first-order quantities (Cruz-Orive, 1989). However, structures

are geometrically not fully characterized by a collection of first-order quantities. For example, two random sets may have the same mean volume fraction V_V, but possess different arrangements in space, due to different *second-order properties*. The aim of the present study consisted in the exploration of the spatial arrangement of the epithelial volume component of normal prostatic tissue and adenocarcinomas of the prostate by *second-order stereology* (Cruz-Orive, 1989; Jensen et al., 1990; Mattfeldt et al., 1993).

MATHEMATICAL BACKGROUND

We consider stationary and isotropic ergodic random closed sets Ξ with positive volume fraction in an unbounded three-dimensional reference space, which will be denoted as *volume processes*. Pairs of points x, $(x + \mathbf{r})$, separated by the line $\mathbf{r}$ with known length r, are thrown into the reference space with uniform random location. The *covariance* $C(r)$ of Ξ is the probability P that two points, which are a distance r apart and both hit the reference space, lie simultaneously in Ξ:

$$C(r) = P[\{x \in \Xi\} \wedge \{(x + \mathbf{r}) \in \Xi\}] \tag{1}$$

The covariance of Ξ may be unbiasedly estimated stereologically from sections (Fig. 1; see Stoyan et al., 1987). One throws pairs of points with growing distance r onto the section. For each distance r one counts the number of pairs N_{11} whose points lie both in Ξ, and the total number of pairs $N_{..}$ whose points lie both in the reference space, not necessarily in Ξ:

$$\hat{C}(r) = N_{11}/N_{..} \tag{2}$$

With an unbiased estimate of the mean volume fraction V_V it is now possible to estimate three other interesting functions of stochastic geometry consistently, namely the *correlation function* $k(r)$, the *pair correlation function* $g(r)$, and the *radial distribution function* $RDF(r)$ (König & Stoyan, 1986; Stoyan et al., 1987; Cruz-Orive, 1989; Ohser, 1991):

$$\hat{k}(r) = \{\hat{C}(r) - (\hat{V}_V)^2\}/\{\hat{V}_V - (\hat{V}_V)^2\} \tag{3}$$

$$\hat{g}(r) = \hat{C}(r)/\{(\hat{V}_V)^2\} \tag{4}$$

$$\widehat{RDF}(r) = 4\pi r^2 \hat{C}(r)/\hat{V}_V \tag{5}$$

The function $\hat{k}(r)$ can be considered as an estimator of the coefficients of autocorrelation as a function of distance r. The pair correlation function $g(r)$ represents the mean volume content of Ξ in a spherical shell of radii r and $r + dr$, centred at a typical point of Ξ, divided by the mean volume content of Ξ in a spherical shell of the same size but centred at an arbitrary point of the reference space (Cruz-Orive, 1989). The function $RDF(r)$ is linked to the *reduced second moment function* $K(r)$ by the relation $RDF(r) = V_V \frac{dK(r)}{dr}$ (Stoyan et al., 1987). If we evaluate $C(r)$ for n growing radii r_i with constant increment Δr, we obtain the following estimator of $K(r)$, in a discretized version, by substituting into eq. (5) (Mattfeldt et al., 1993):

$$\hat{K}(r_i) = (4\pi/\hat{V}_V^2) \sum_{i=1}^{r_i/\Delta r} r_i^2 \hat{C}(r_i)\Delta r; \quad i = 1, ..., n \tag{6}$$

For volume processes, $K(r)$ denotes the ratio of the mean measure of Ξ in a volume of a sphere of radius r, centred at a typical point of Ξ, to the volume density of Ξ

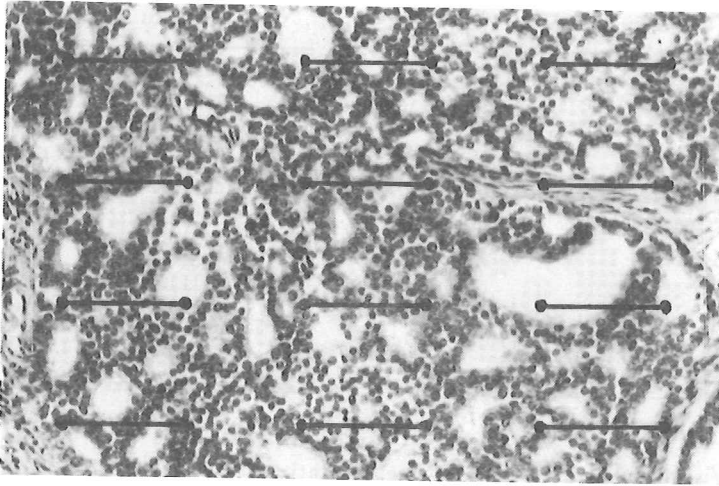**Fig. 1.** A visual field from a prostatic adenocarcinoma with $N_{..} = 12$ dipoles of length $r = 100$ μm. The number of dipoles whose endpoints *both* hit epithelium is $N_{11} = 8$, hence $\hat{C}(100 \ \mu m) = 8/12 = 2/3$. To obtain more values of $\hat{C}(r)$, the evaluation is repeated for dipoles of other lengths r.

(Cruz-Orive, 1989). Eq. (6) is a new estimator of $K(r)$ for volume processes with edge effects implicitly corrected. Finally, we consider a hypothetical, "completely random" volume process of intensity V_V, where every test point would be marked uniformly at random and independently as "1" with probability V_V, and as "0" with probability $(1 - V_V)$. For such a process, we would have the *reference functions* $C_{ref}(r) = V_V^2$, hence $RDF_{ref}(r) = 4\pi r^2 V_V$, $k_{ref}(r) = 0$, $g_{ref}(r) = 1$, and $K_{ref}(r) = (4\pi/3)r^3$ for all $r > 0$ (Mattfeldt et al., 1993). When estimated functions from real samples are available, they can be compared to these reference functions in order to test whether there is *interaction* — *clustering* or *repulsion* — within the empirical structure for the explored distance range. Note that the reference functions for $C(r)$ and $RDF(r)$ depend on V_V, whereas for $k(r)$, $g(r)$ and $K(r)$ they do not depend on V_V.

MATERIALS AND METHODS

Twenty radical prostatectomy specimens from patients with invasive prostatic adenocarcinoma were investigated. Ten visual fields per case were sampled systematically from tumour tissue and from tumour-free domains in each specimen using paraffin sections stained with haematoxylin and eosin. The selected fields were transmitted to an image analyzer with a black-and-white CCD camera. The result was a gray level image with a resolution of 512×512 pixels. By interactive segmentation a binary image was produced, where pixels with the epithelial component were coded as 1, and the pixels with non-epithelial components were coded as 0. An array of 32×32 pixels per image was used for the further evaluations (Fig. 2a,b). First, V_V was estimated according to the principle of Delesse. For the estimation of $C(r)$ from an image, the distances r between *all* pairs of different points of the array were calculated. The distances were classified into 32 groups with an interval length of $\Delta r = 13.6$ μm from $r = 0$ to $r = 435.2$ μm. Then the quantities N_{11} and $N_{..}$ were determined for each class of distances, and the

Case 7: Image 1   Case 16: Image 9

Tumour–free   Carcinoma
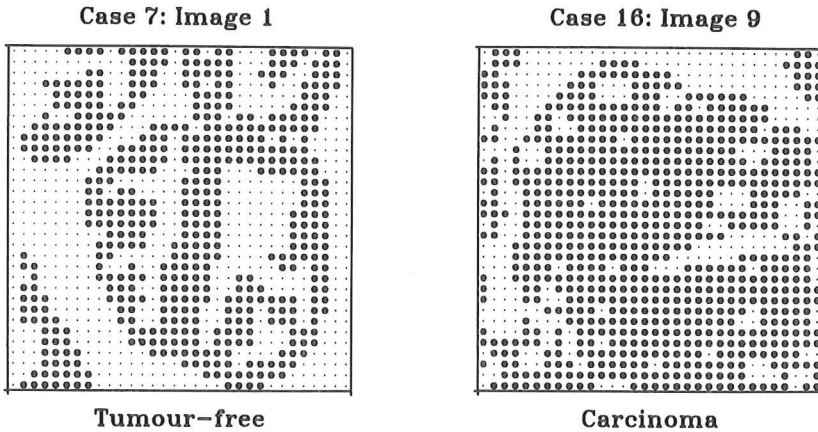
Fig. 2. Visual fields from tumour-free prostatic tissue (left panel) and a prostatic adenocarcinoma (right panel) were first digitized as images of 512×512 pixels. These images were reduced to 32×32 pixels for the automatic estimation of $C(r)$ and V_V. Heavy dots: epithelium, light dots: non-epithelial components. Intact glandular architecture (left) and dedifferentiation (right) are recognizable despite considerable loss of information as compared to the original image in the microscope (no colour, binary image instead of gray values, only 1/256 of all pixels).

mean function of $\hat{C}(r)$ was estimated for each case according to eq. (2) after averaging $\hat{C}(r)$ between images within cases separately for each class. By substituting the mean values of $C(r)$ and V_V per case into eqs. (3–6), the other functions were estimated. For group comparisons, means and 95%-confidence intervals were calculated within the 2 groups from the mean functions of the cases using the t-distribution.

RESULTS AND DISCUSSION

The mean volume fraction of the epithelial component was significantly higher in adenocarcinomas (mean $= 0.62$, $SD = 0.09$) than in tumour-free prostatic tissue (mean $= 0.41$, $SD = 0.08$, $P < 0.0001$). The functions $\hat{C}(r)$ and $\widehat{RDF}(r)$ (Fig. 3a, b) differed considerably between tumour-free and cancerous tissue, but these functions depend on spatial pattern *and* V_V. As carcinomatous tissue had a higher epithelial volume fraction V_V than tumour-free tissue, their estimation did not permit a safe distinction between different types of spatial arrangement. Analysis of the functions $\hat{k}(r)$, $\hat{g}(r)$, and $\hat{K}(r)$, which are *not* dependent on V_V, showed clustering of epithelial volume at short distances, and repulsion of epithelial volume at long distances (Fig. 3c,d, Fig. 4a). Glandular epithelium consists of cell groups, which implies clustering at short distance ranges; it also develops glandular openings (lumina) and is surrounded by stromal components, which implies repulsion at longer distances. The best distinction between benign and malignant tissue was obtained by estimation of $g(r)$, which showed a partial loss of short-range and long-range interaction in the carcinomatous tissue (Fig. 4a). The low interindividual scatter of $\hat{k}(r)$, $\hat{g}(r)$ and $\hat{K}(r)$ indicates a high biological significance of spatial pattern. Fig. 4b displays the mean pair correlation functions for acinar and cribriform prostatic adenocarcinomas. For acinar adenocarcinomas, $\hat{g}(r)$ showed
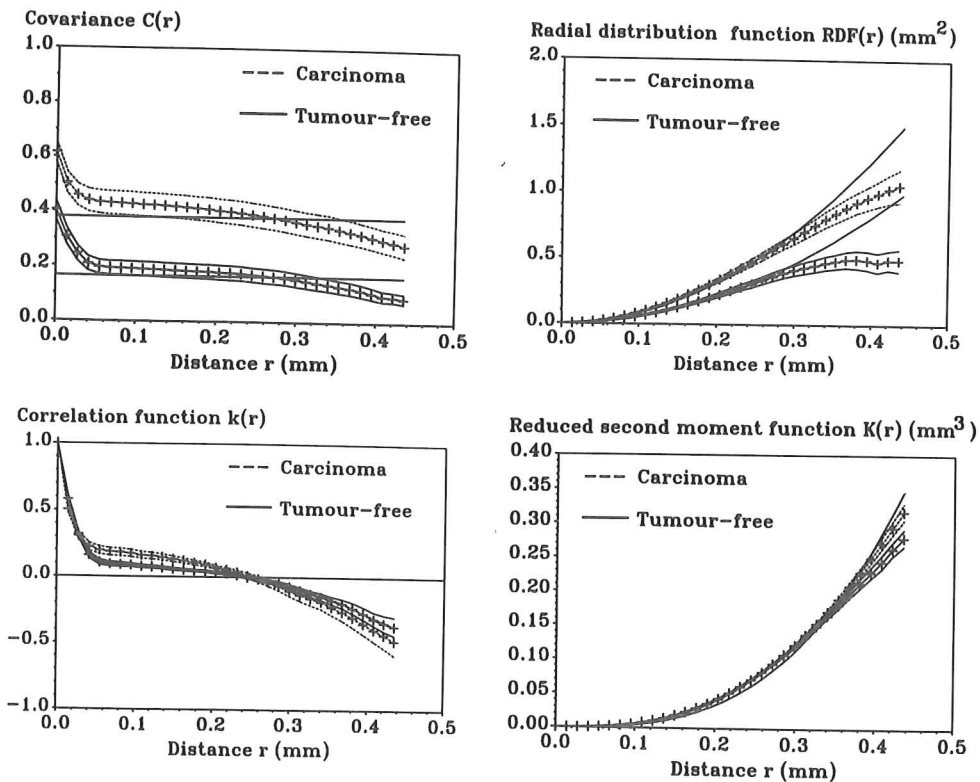
Fig. 3a (left upper panel). Plot of the mean covariances $\hat{C}(r)$ (indicated by crosses) with 95%-confidence intervals for tumour-free prostatic tissue and prostatic adenocarcinomas. Upper horizontal line: reference curve for carcinomas $C_{ref} = 0.62^2$, lower horizontal line: reference curve for tumour-free tissue $C_{ref} = 0.41^2$. **Fig. 3b** (right upper panel). Plot of the mean radial distribution functions $\widehat{RDF}(r)$. Upper continuous curve: reference curve for carcinomas $RDF_{ref} = (4\pi r^2)0.62$, lower continuous curve: reference curve for tumour-free tissue $RDF_{ref} = (4\pi r^2)0.41$. **Fig. 3c** (left lower panel). Plot of the correlation functions $\hat{k}(r)$ for tumour-free tissue and prostatic adenocarcinomas. The horizontal line is the reference curve $k_{ref} = 0$ for both groups. **Fig. 3d** (right lower panel). Plot of the reduced second moment functions $\hat{K}(r)$ for tumour-free prostatic tissue and prostatic adenocarcinomas. The polynomial $K_{ref} = (4\pi/3)r^3$ is the reference curve for both groups. The variance between cases is exceedingly low (confidence intervals hardly visible).

a steeper initial descent near $r = 0$ than for cribriform carcinomas, which agrees well with the widely held view that the acinar carcinomas are better differentiated than the cribriform tumour type. To examine the diagnostic accuracy in individual cases, the specimens 1–10 were used as a *learning set*, from which the computer had to "learn" to distinguish between tumour-free tissue and carcinomatous tissue using $\hat{g}(r)$. When the learnt criteria were then applied to the *test set*, i.e. the cases 11–20, all samples
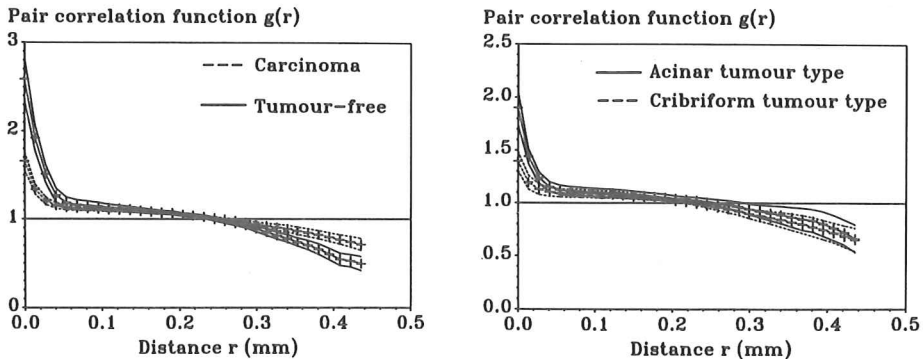
Fig. **4a** (left panel). Plot of the mean pair correlation functions $\hat{g}(r)$ (indicated by crosses) with 95%-confidence intervals for tumour-free prostatic tissue and prostatic adenocarcinomas. The horizontal line is the reference curve $g_{ref} = 1$ for both groups. No overlap of confidence intervals at short and long distances r. **Fig. 4b** (right panel). Plot of the mean pair correlation functions $\hat{g}(r)$ for acinar prostatic and cribriform prostatic adenocarcinomas. Note steeper initial descent of $\hat{g}(r)$ for the acinar tumours.

were diagnosed correctly. The differences between normal and carcinomatous prostatic tissue were very similar to those between mastopathy and invasive ductal breast cancer, which were reported recently (Mattfeldt et al., 1993). Thus, second-order stereology reproducibly detects architectural differences between benign and malignant glandular tissue, with $g(r)$ serving as the most useful tool.

ACKNOWLEDGMENT

REFERENCES

Cruz-Orive L.-M. Second-order stereology: estimation of second moment volume measures. Acta Stereol 1989; 8:641–646.

Jensen EB, Kiêu K, Gundersen HJG. Second-order stereology. Acta Stereol 1990; 9:15–35.

König D, Stoyan D. Second-order moments in stereological study of random forms. Sci. Form 1986; 2:21–35.

Mattfeldt T, Frey H, Rose C. Second-order stereology of benign and malignant alterations of the human mammary gland. J Microsc 1993; 171:143–151.

Ohser J. On estimation of pair correlation functions. Res Inform 1991; 4:147–152.

Stoyan D, Kendall WS, Mecke J. Stochastic Geometry and Its Applications. Chichester: Wiley, 1987:183–186.